Journal of Thrombosis and Haemostasis, **16**: 352–363 DOI: 10.1111/jth.13875

IN FOCUS

The small-molecule MERTK inhibitor UNC2025 decreases platelet activation and prevents thrombosis

B. R. BRANCHFORD,*† T. J. STALKER,‡ L. LAW,* G. ACEVEDO,* S. SATHER,* C. BRZEZINSKI,* K. M. WILSON,§ K. MINSON,¶** A. B. LEE-SHERICK,* P. DAVIZON-CASTILLO,* C. NG,*† W. ZHANG,†† K. B. NEEVES,‡‡ S. R. LENTZ,§ X. WANG,†† S. V. FRYE,††§§ H. SHELTON EARP III,§§¶¶ D. DERYCKERE,¶** L. F. BRASS,‡ D. K. GRAHAM¶** and J. A. DI PAOLA*†***

**Department of Pediatrics, Section of Hematology/Oncology, University of Colorado School of Medicine; †University of Colorado Hemophilia and Thrombosis Center, Aurora, CO; ‡Department of Medicine, University of Pennsylvania, Philadelphia, PA; §Carver College of Medicine, University of Iowa, Iowa City, IA; ¶Aflac Cancer and Blood Disorders Center of Children's Healthcare of Atlanta; **Department of Pediatrics, Section of Hematology/Oncology, Emory University School of Medicine, Atlanta, GA; ††Center for Integrative Chemical Biology and Drug Discovery, Division of Chemical Biology and Medicinal Chemistry, Eshelman School of Pharmacy, University of North Carolina, Chapel Hill, NC; ‡‡Department of Chemical & Biological Engineering, Colorado School of Mines, Golden, CO; §§Lineberger Comprehensive Cancer Center, Department of Medicine, School of Medicine, University of North Carolina; ¶¶Department of Pharmacology, University of North Carolina at Chapel Hill, Chapel Hill, NC; and ***Graduate Program – Human Medical Genetics, University of Colorado School of Medicine, Aurora, CO, USA*

To cite this article: Branchford BR, Stalker TJ, Law L, Acevedo G, Sather S, Brzezinski C, Wilson KM, Minson K, Lee-Sherick AB, Davizon-Castillo P, Ng C, Zhang W, Neeves KB, Lentz SR, Wang X, Frye SV, Shelton Earp H III, DeRyckere D, Brass LF, Graham DK, Di Paola JA. The small-molecule MERTK inhibitor UNC2025 decreases platelet activation and prevents thrombosis. *J Thromb Haemost* 2018; **16**: 352–63.

See also Cosemans JMEM. At the MERcy of platelet primers. This issue, pp 349–51.

Essentials

- Signaling by Gas6 through Tyro3/Axl/Mer receptors is essential for stable platelet aggregation.
- UNC2025 is a small molecule inhibitor of the Mer tyrosine kinase.
- UNC2025 decreases platelet activation *in vitro* and thrombus formation *in vivo*.
- UNC2025's anti-platelet effect is synergistic with inhibition of the ADP receptor, $P2Y_{12}$.

Summary. *Background:* Growth arrest-specific protein 6 signals through the TAM (TYRO-3–AXL–MERTK) receptor family, mediating platelet activation and thrombus formation via activation of the aggregate-stabilizing $\alpha_{IIb}\beta_3$ integrin. *Objective:* To describe the antithrombotic effects mediated by UNC2025, a small-molecule MERTK tyrosine kinase inhibitor. *Methods:* MERTK phosphorylation and downstream signaling were assessed by immunoblotting. Light transmission aggregometry, flow cytometry and microfluidic analysis were used to evaluate the impact of MERTK inhibition on platelet activation and stability of aggregates *in vitro*. The effects of MERTK inhibition on arterial and venous thrombosis, platelet accumulation at microvascular injury sites and tail bleeding times were determined with murine models. The effects of combined treatment with ADP–$P2Y_{1\&12}$ pathway antagonists and UNC2025 were also evaluated. *Results and Conclusions:* Treatment with UNC2025 inhibited MERTK phosphorylation and downstream activation of AKT and SRC, decreased platelet activation, and protected animals from pulmonary embolism and arterial thrombosis without increasing bleeding times. The antiplatelet effect of UNC2025 was enhanced in combination with ADP–$P2Y_{1\&12}$ pathway antagonists, and a greater than additive effect was observed when these two agents with different mechanisms of inhibition were coadministered. TAM kinase signaling represents a potential therapeutic target, as inhibition of this axis, especially in combination with ADP–P2Y pathway antagonism, mediates decreased platelet activation, aggregate stability, and thrombus formation, with less hemorrhagic potential than current treatment strategies. The data presented here also demonstrate antithrombotic activity mediated by UNC2025, a novel

Correspondence: Jorge Di Paola, University of Colorado School of Medicine and Children's Hospital Colorado, Department of Pediatrics, Hematology/Oncology/BMT, 12800 E. 19th Ave, Mail Stop 8302, Building RC-1 North, Aurora, CO 80045, USA
Tel.: +1 303 724 4000
E-mail: jorge.dipaola@ucdenver.edu

Received: 25 June 2016
Manuscript handled by: J. Heemskerk
Final decision: P. H. Reitsma, 3 September 2017

translational agent, and support the development of TAM kinase inhibitors for clinical applications.

Keywords: growth arrest-specific protein 6; integrin $\alpha_{IIb}\beta_3$; MERTK; platelet activation; thrombosis.

Introduction

Stable platelet aggregation is essential for adequate hemostasis, but uncontrolled platelet activation may lead to life-threatening thromboses such as arterial ischemic stroke or myocardial infarction. Current antiplatelet therapies are complicated by hemorrhagic side effects and interpatient response variability [1], demonstrating the need to explore new pathways that may yield safer and more effective therapies.

Extracellular growth arrest-specific protein 6 (GAS6) stimulates the platelet surface TYRO-3–AXL–MERTK (TAM) family of transmembrane receptor tyrosine kinases [2–6] to dimerize and autophosphorylate [7–9], activating phosphatidylinositol 3-kinase (PI3K) [10,11], RAP1 [11–13], and AKT [14,15], thereby triggering β_3 integrin phosphorylation and amplifying outside-in signaling [2,16,17]. GAS6 has been reported in human platelets and plasma [3,5,18], and bridges membrane-bound phosphatidylserine [19,20] and TAM kinases [21,22].

Inhibition or absence of GAS6 or any TAM receptor decreases platelet aggregation and impairs thrombus formation [2,3,23,24]. *Gas6*$^{-/-}$ mice form unstable platelet aggregates that are stabilized by the addition of recombinant human GAS6 [5]. GAS6 enhances PI3K phosphorylation in platelets from wild-type mice, but not in platelets from *Tyro3*$^{-/-}$, *Mertk*$^{-/-}$ or *Axl*$^{-/-}$ mice [2]. Interestingly, absence of GAS6–TAM signaling does not increase spontaneous hemorrhage or bleeding time after tail clipping [2–4, 6,25].

Here, we describe a novel mechanism of GAS6–TAM signal inhibition in platelets, targeting the MERTK tyrosine kinase active site with a highly potent and bioavailable MERTK inhibitor, UNC2025 [26–29].

Materials and methods

Platelet activation inhibitors

1 UNC2025*: MERTK inhibitor synthesized as described [26]. The molecular structure is shown in Fig. S1. The half-life of UNC2025 is 3.8 h in mice, with low clearance (9.2 mL min^{-1} kg^{-1}) and 100% oral bioavailability. A 3 mg kg^{-1} dose results in a C_{max} of □ 22 nM at 30 min [26].*
2 PBS0739*: $P2Y_{12}$ receptor antagonist (Tocris, Bristol, UK).*
3 MRS2179*: $P2Y_1$ receptor antagonist (Tocris).*
4 2-MeSAMP*: $P2Y_{12}$ receptor antagonist (Sigma-Aldrich, St Louis, MO, USA).*

In some cases, MRS2179 and 2-MeSAMP were used together, and are collectively referred to as P2Y receptor inhibitor (P2Yi).

Blood collection

Human whole blood (WB) was collected by venipuncture from healthy volunteers after informed consent had been obtained under an Institutional Review Board-approved protocol.

Washed platelet (WP) and platelet-rich plasma (PRP) preparation

WB was drawn from healthy volunteers into 3.8% sodium citrate, with addition of acid–citrate–dextrose [30,31]. WPs and PRP were prepared as described previously [32].

Platelet aggregation

Human WPs or PRP, or murine WPs, were incubated for 15 min with saline (vehicle), 0.5 μM (WPs) or 5 μM (PRP) UNC2025, 0.001 μM PBS0739 ($P2Y_{12}$ receptor inhibitor), or 2 μM abciximab (positive control). Samples were analyzed by light transmission aggregometry after stimulation with 1 μg mL^{-1} (WPs) or 2 μg mL^{-1} (PRP) collagen, 50 ng mL^{-1} convulxin, 2 μM ADP, or 1 U mL^{-1} thrombin. Maximum aggregation (%) was recorded.

Flow cytometry

Human WPs were incubated for 15 min with saline (vehicle), 0.5 μM UNC2025, or 2 μM abciximab, and then stimulated with 50 ng mL^{-1} convulxin (Santa Cruz Biotechnology, Santa Cruz, CA, USA). PAC-1 antibodies (BD Biosciences, San Jose, CA, USA) were added immediately after convulxin, samples were incubated for 5 min, and platelets were fixed with 2% paraformaldehyde (Sigma-Aldrich). Samples were analyzed with a Gallios flow cytometer (Beckman-Coulter, Indianapolis, IN, USA). Mean fluorescence intensity was recorded.

Microfluidic flow assay

Microfluidic experiments were performed on a collagen surface [33–35]. WB (100 μL) was incubated for 1 min with saline (vehicle), 1 μM UNC2025, or 2 μM abciximab (positive control), and then pulled through the channels for 3 min at a physiologic wall shear rate (650 s^{-1}). Platelet adhesion and aggregation were captured in real time with an ORCA Flash4 CMOS camera (Orca-ER; Hamamatsu, Hamamatsu City, Japan) and CELLSENSE imaging software (Olympus Life Science, Center Valley, PA, USA), with images being acquired every 1 s over the duration of the experiment. Surface area coverage and aggregate size were determined for each series.

Immunoblotting Human WPs were incubated with UNC2025 or saline vehicle at 37 °C for 5 min, stimulated with 1 μg mL^{-1} collagen, and resuspended in lysis buffer containing 50 mM HEPES (pH 7.5), 150 mM NaCl, 10 mM EDTA, 10% (v/v) glycerol, 1% (v/v) Triton X-100, 1 mM sodium orthovanadate, 0.1 mM sodium molybdate, and protease inhibitors (Roche Diagnostics, Indianapolis, IN, USA). Lysates were incubated on ice for 15–20 min, and the protein supernatant was collected after centrifugation at 3381 × *g* for 3 min. For MERTK detection, cells were treated with 120 μM pervanadate for 3 min prior to cell lysis to stabilize phosphoproteins. Lysates were incubated overnight with anti-MERTK antibody (MAB8912; R&D Systems, Minneapolis, MN, USA) and rec-protein G–sepharose beads (Invitrogen, Carlsbad, CA, USA), and bound proteins were eluted into 2 × Laemmli sample buffer (Bio-Rad, Hercules, CA, USA). WP lysates or immunoprecipitated proteins were resolved by electrophoresis on 8% Tris-glycine SDS polyacrylamide gels (Invitrogen), and transferred onto nitrocellulose membranes. Membranes were blocked in Tris-buffered saline with 0.1% Tween-20 and 5% milk. The following antibodies were used for immunoblot analysis according to the manufacturers' recommendations: anti-phospho-MERTK (Phosphosolutions, Aurora, CO, USA), anti-MERTK (ab52968; AbCam, Cambridge, UK), anti-phospho-AKT (Ser473, #92715), anti-AKT (#9272S), anti-phospho-SRC (Y416, #2101S), anti-SRC (#2109S) (Cell Signaling, Danvers, MA, USA), and anti-actin (#sc-1616; Santa Cruz Biotechnology). Proteins were detected by horseradish peroxidase (HRP) chemiluminescence (Perkin-Elmer, Waltham, MA, USA) with goat anti-rabbit IgG–HRP secondary antibody (#170-6515; Bio-Rad).

Murine models All experiments were approved by university animal care and use committees, and involved equal numbers of 6–12-week-old male and female C57BL/6J mice (Jackson Laboratories, Bar Harbor, ME, USA).

$FeCl_3$-induced carotid artery thrombosis

Mice were anesthetized and subjected to endotracheal intubation and mechanical ventilation [36–39]. After carotid artery exposure and ultrasonic flow probe attachment, saline vehicle, 3 mg kg^{-1} UNC2025, high-dose (HD) P2Yi (3 mg kg^{-1} each of MRS2179 and 2-MeSAMP), low-dose (LD) P2Yi (1.5 mg kg^{-1} each of MRS2179 and 2-MeSAMP) or UNC2025 + LD P2Yi was intravenously injected and allowed to circulate for 30 min. Six per cent $FeCl_3$ was applied to the artery for 3 min, and the probe readout was captured for 60 min after $FeCl_3$ application. Elapsed time to first (initial) artery occlusion (TTFO) (mean blood flow of 0 mL min^{-1} for > 30 s), and total duration of occlusion (DOO) (mean blood flow < 20% of pre-$FeCl_3$ baseline) were determined.

Pulmonary embolism (PE)

Mice were treated for 30 min with 3 mg kg^{-1} UNC2025 or saline vehicle administered by intravenous injection, and type 1 equine fibrillar collagen (0.28 mg kg^{-1}) and epinephrine (0.029 mg kg^{-1}) were then administered, and time to breathing cessation was recorded as described previously [24,38]. Mice that remained alive 15 min after collagen/epinephrine administration were killed, and experimental time was recorded as 15 min.

Intravital microvascular thrombosis

Mice underwent intravital microscopy of the cremaster muscle microcirculation [40,41]. Arterioles 30–40 μm in diameter with unperturbed blood flow were studied. After a 10-min stabilization period, labeled anti-CD41 $F(ab)_2$ fragments (0.12 μg g^{-1} body weight), anti-P-selectin (0.2 μg g^{-1}) and anti-fibrin (0.2 μg g^{-1}) were intravenously infused. Vascular injury was induced by pulsed nitrogen dye laser (NL100, 440 nm; Stanford Research Systems, Sunnyvale, CA, USA), and up to five injuries and thrombi were recorded in each mouse following saline infusion. Next, 3 mg kg^{-1} UNC2025 was infused and allowed to circulate for 30 min, and a second set of injuries/thrombi were recorded. CD41, P-selectin and fibrin were measured by summing all pixels in a frame with the corresponding fluorescence intensity above background.

Murine tail bleed assay

Saline vehicle, 3 mg kg^{-1} UNC2025, HD P2Yi (3 mg kg^{-1} each of MRS2179 and 2-MeSAMP), LD P2Yi (1.5 mg kg^{-1} each of MRS2179 and 2-MeSAMP) or UNC2025 + LD P2Yi was injected into the retro-orbital sinus and allowed to circulate for 15 min. Tails were snipped 1 cm from the tip, and the proximal ends were placed in a conical tube containing 37 °C normal saline for 15 min. Total bleeding time (including rebleeds) was recorded [37,38].

Synergy calculations

Median effect analysis was performed according to the methods of Chou and Talaly [42] with Calcusyn software (Calcusyn, Cambridge, UK). Interactions were also assessed with the Bliss additivity equation $Fa_{12} = fa_1 + fa_2 - fa_1 \times fa_2$, where fa = frequency of effect mediated by drug 1 or 2, respectively, and Fa_{12} = predicted frequency of effect for an additive interaction. An observed Fa greater than the calculated Fa_{12} indicates synergy.

Statistical analyses

Data with a Gaussian distribution are expressed as mean ± standard error of the mean (SEM), with

significance evaluated with paired, two-tailed *t*-tests. Data with a non-normal non-Gaussian distribution are expressed as median ± interquartile range (IQR), and were evaluated with Mann–Whitney rank sum tests. Experiments with human WB, PRP or WPs were performed and analyzed as paired samples. Murine assays were analyzed as unpaired samples.

Results

UNC2025 decreased platelet MERTK phosphorylation and downstream signaling

UNC2025 caused dose-dependent inhibition of MERTK phosphorylation in unstimulated human platelets and after stimulation with collagen (Fig. 1A). In this context, treatment with 0.5 μM UNC2025 resulted in partial inhibition of MERTK, and a dose of 5 μM was sufficient for more complete inhibition. Signaling through the AKT and SRC pathways, which are known downstream targets of MERTK, was similarly descreased in platelets treated with UNC2025 (Fig. 1B). These data demonstrate the utility of UNC2025 as a MERTK inhibitor in human platelets, and define the dose of UNC2025 required for effective MERTK inhibition.

UNC2025 decreased human and murine platelet activation

UNC2025 caused dose-dependent decreases in mean (± SEM) maximum aggregation of human platelets stimulated with collagen, ADP, or thrombin (Fig 2A,B; Fig. S2). Treatment with 0.5 μM UNC2025 decreased mean (± SEM) maximum collagen-stimulated aggregation of human WPs (18.0% ± 9.8%, $n = 6$, $P < 0.05$) as compared with saline-treated controls (54.0% ± 8.7%, $n = 6$) (Fig. 2A). Similarly, Fig. 2B demonstrates decreased collagen-stimulated aggregation of human PRP pretreated with 5 μM UNC2025 (36.9% ± 12.0%, $n = 7$, $P < 0.05$) as compared with saline-treated controls (75.7% ± 8.7%, $n = 7$). Pretreatment with 2 μM abciximab is shown as a positive control. Finally, treatment with 0.5 μM UNC2025 also caused decreased collagen-stimulated aggregation of murine WPs (37.3% ± 5.7%, $n = 10$, $p < 0.01$) as compared with saline-treated controls (58.2% ± 5.8%, $n = 20$) (Fig. S3).

As both GAS6–TAM and ADP–P2Y signaling axes involve PI3K-mediated activation of integrin $\alpha_{IIb}\beta_3$, we next studied the nature of platelet inhibition and thrombosis protection after antagonism of both of these pathways. Treatment with 0.5 μM UNC2025 or 0.001 μM PBS0739, a $P2Y_{12}$ inhibitor, caused decreased collagen-induced aggregation of human WPs, and the effect of combined treatment was more than additive, according to analyses with both the Chou–Talaly and Bliss independence models (Fig. 2C; Fig. S4). The mean maximum collagen-induced aggregation in samples treated with 0.5 μM UNC2025 (55.0% ± 1.7%, $n = 6$, $P < 0.001$) or 0.001 μM PBS0739 (64.1% ± 2.3%, $n = 6$, $P < 0.05$) differed significantly from that in saline-treated negative controls (70.3% ± 1.2%, $n = 6$). Samples treated with a

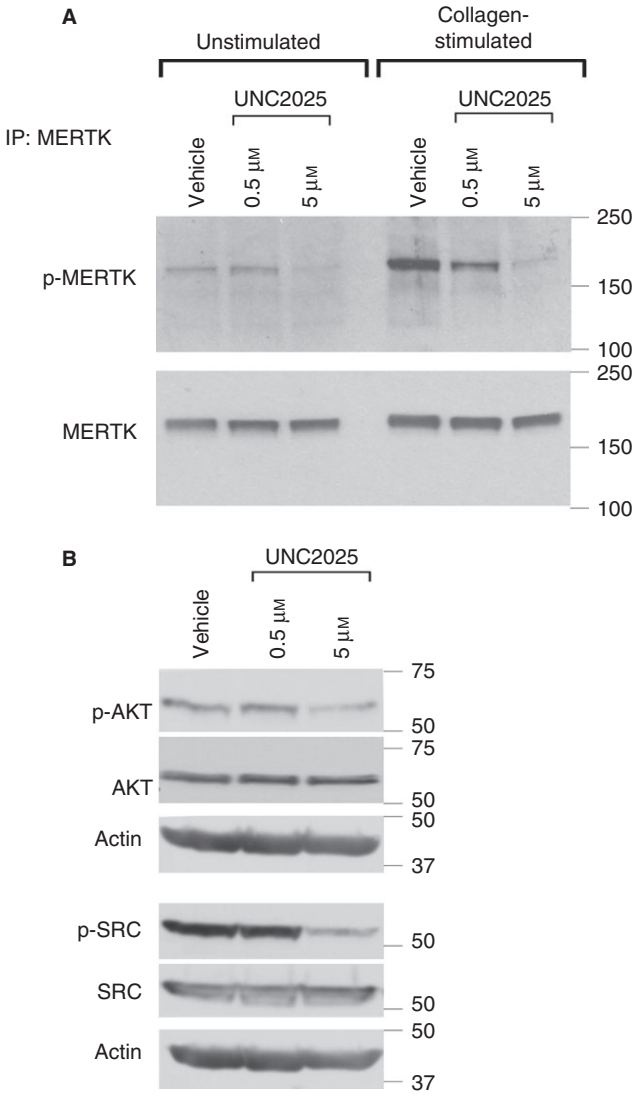

Fig. 1. UNC2025 inhibits phosphorylation of MERTK and downstream signaling proteins in a dose-dependent manner. (A) Freshly prepared human washed platelets were treated with the indicated concentrations of UNC2025 or vehicle, and then stimulated with 1 μg mL^{-1} collagen or left unstimulated. Lysates were prepared, MERTK was immunoprecipitated, and levels of phosphorylated MERTK (p-MERTK) and total MERTK were detected by immunoblotting. Collagen-stimulated samples showed greater phosphorylation of MERTK than unstimulated controls. Dose-dependent inhibition of MERTK phosphorylation was evident under both conditions in response to treatment with UNC2025. Levels of total MERTK were unchanged. (B) Human platelets were treated with the indicated concentrations of UNC2025 or vehicle, and lysates were prepared. Immunoblot analysis demonstrated dose-dependent inhibition of phosphorylated AKT (p-AKT) and phosphorylated SRC (p-SRC). Total AKT and SRC levels were unchanged. Actin is shown as a loading control. Images are representative of at least three independent experiments. IP, immunoprecipitation.

combination of PBS0739 and UNC2025 had significantly decreased mean maximum aggregation (38.3% ± 4.4%, $n = 6$) as compared with samples treated with saline ($P < 0.001$), UNC2025 alone ($P = 0.006$), or PBS0739 alone ($P = 0.002$). The combination index was determined on the basis of the Chou–Talaly model, and was < 1, indicating synergy [42]. According to the Bliss additivity equation, a mean (± SEM) 31% ± 7.2% decrease in platelet aggregation was predicted for an additive interaction, but significantly greater inhibition (61% ± 8.8%, $P = 0.02$) was observed, indicating synergistic inhibition of platelet aggregation mediated by the two compounds.

UNC2025 decreases activation of $\alpha_{IIb}\beta_3$

Next, we studied the effects of UNC2025 on activation of human WPs as indicated by P-selectin expression (anti-P-selectin antibody binding) and conformational change of β_3 integrin (PAC-1 binding). Samples treated with 0.5 μM UNC2025 showed decreased mean fluorescence intensity (± standard error) of PAC-1 binding (respectively: 1.3 ± 0.3 units, $P < 0.005$; and 0.16 ± 0.03 units, $P < 0.01$) as compared with controls pretreated with an equivalent volume of saline (1.9 ± 0.26 units, $n = 5$) (Fig. 2D). There was no significant difference in P-selectin expression (Fig. S5) between groups. The lack of changes in anti-P-selectin antibody binding suggests that α-granule release was not affected by treatment with UNC2025.

UNC2025 reduced human platelet aggregate stability under flow conditions

The impact of UNC2025-mediated MERTK inhibition on platelet aggregate formation in human WB was evaluated under physiologic flow conditions, with a microfluidic model [35,43]. At the end of each WB perfusion (and buffer rinse), platelet aggregates showed decreased surface area coverage in samples treated with 0.5 μM UNC2025 as compared with saline-treated samples (Fig. 3A,B). The surface area covered by platelet aggregates increased over time in all samples, but the increase was more pronounced after saline treatment than after treatment with UNC2025 or abciximab. Smaller aggregates were observed at the end of the run in UNC2025-treated samples, and disaggregation of large aggregates was directly visualized during the run and occurred more often in UNC2025-treated samples than in saline-treated samples. Review of the surface area coverage accumulation over time revealed a trend towards greater mean (± standard error) numbers of aggregate embolizations under flow conditions in samples pretreated with UNC2025 (8.1 ± 3.2) than in controls pretreated with saline, although this difference did not reach statistical significance (4.0 ± 0.9, P = not significant [NS]). Mean (± standard error) surface area coverage at the end of the run (after buffer rinse) was significantly decreased in UNC2025-treated samples ([10.0 ± 5.1] × 10^4 pixels) as compared with saline-treated controls ([44.5 ± 13.9] × 10^4 pixels, $n = 5$, $P < 0.05$), as seen in Fig. 3C. Thus, MERTK inhibition decreased platelet aggregate stability under flow conditions.

After 300 s, samples pretreated with UNC2025 showed a decreased area under the curve ([12.5 ± 1.5] × 10^4 pixels) as compared with saline-treated controls ([37.4 ± 2.8] × 10^4 pixels), and the area under the curve was similar to that of samples pretreated with the positive control abciximab ([2.6 ± 0.2] × 10^4 pixels) (Fig. 3D).

UNC2025 decreased platelet activation at murine microcirculation vascular injury sites

Next, we used an *in vivo* murine microcirculation thrombosis model to allow better characterization of clot regional architecture-specific effects. Treatment with 3 mg kg^{-1} UNC2025 caused significant decreases in median peak area for total/CD41-positive (384 μm^2, IQR 113–97 μm^2, $P = 0.013$) and activated/P-selectin-positive (81 μm^2, IQR 18–149 μm^2, $P = 0.047$) platelets at sites of laser-induced vascular injury in the mouse cremaster muscle microcirculation, as compared with saline-treated controls (respectively: 822 μm^2, IQR 485–1596 μm^2; and 117 μm^2, IQR 89–174 μm^2), but fibrin accumulation was not affected (respectively: 134 μm^2, IQR 88–239 μm^2; and 162 μm^2, IQR 95–239 μm^2) (Fig. 4). Video S1A and Video S1B show the increase in total and activated platelet accumulation at the injury site in saline-treated controls as compared with UNC2025-treated mice, respectively.

UNC2025 decreased murine arterial thrombosis

Next, we evaluated the effects of UNC2025 on larger vessels. Mice pretreated with 3 mg kg^{-1} UNC2025 30 min prior to 6% $FeCl_3$ application to the carotid artery showed prolonged time to initial clot formation (Fig. 5A) and decreased thrombus stability (Fig. 5B) as compared with saline-treated controls. Mean (± SEM) TTFO in saline-treated controls (7.3 ± 0.3 min, $n = 19$) was significantly shorter than that in mice treated with UNC2025 (8.4 ± 0.6 min, $n = 10$, $P = 0.05$) (Fig. 5A). Median DOO, defined as the total time of vessel occlusion during a 60-min experiment, was significantly longer in saline-treated controls (52.3 min, IQR 47.8–53.3 min, $n = 19$) than in UNC2025-treated mice (38.2 min, IQR 9.9–50.1 min, $n = 10$, $P = 0.02$) (Fig. 5B). These results demonstrate that UNC2025-mediated protection of mice from arterial clots is probably attributable, at least in part, to decreased stability of the initial platelet aggregate. Review of the ultrasound probe tracings revealed a trend towards increased mean (± standard error) clot embolizations in mice pretreated with UNC2025 (2.1 ± 1.0 emboli per mouse) as compared with controls

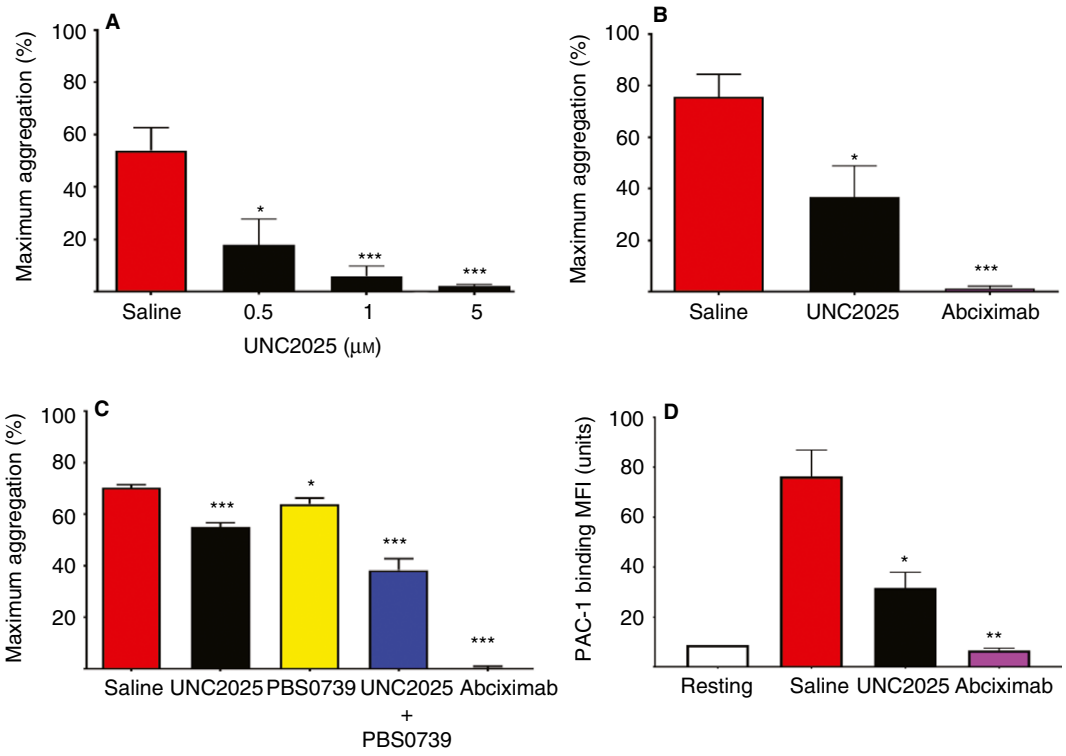

Fig. 2. UNC2025 decreases *in vitro* platelet activation responses. Freshly prepared human washed platelets (WPs) (A, C, D) or platelet-rich plasma (PRP) (B) were treated with the indicated inhibitors or saline vehicle control, and light transmission aggregometry was performed after stimulation with 1 μg mL^{-1} (WPs) (A, C) or 2 μg mL^{-1} (PRP) (B) collagen or 50 ng mL^{-1} convulxin (D). (A) WPs were treated with saline (red bar) or the indicated concentrations of UNC2025 to determine dose–response relationships. (B) PRP treated with 5 μM UNC2025 (black bar) or the positive control 2 μM abciximab (purple) aggregated significantly less than that treated with an equivalent volume of saline (red). (C) WPs treated with a combination (blue bar) of 0.5 μM UNC2025 and 0.001 μM P2Y12 inhibitor (PBS0739) showed synergistic inhibition of aggregation (see also Fig. S4) as compared with platelets treated with 0.5 μM UNC2025 (black) or 0.001 μM PBS0739 (yellow) alone, or with saline (red). (D) Flow cytometric analysis of WPs stimulated with convulxin revealed decreased PAC-1 binding, as indicated by reduced mean fluorescence intensity (MFI, arbitrary units), after pretreatment with 1 μM UNC2025 (black bars) or the positive control abciximab (purple), as compared with saline (red). Mean values ± standard errors derived from five independent donors are shown. Statistics reflect comparison of each experimental condition with the saline vehicle control by the use of Student's *t*-test: $*P < 0.05$, $**P < 0.01$, $***P < 0.001$. [Color figure can be viewed at wileyonlinelibrary.com]

pretreated with saline (0.9 ± 0.5 emboli per mouse, P = NS).

GAS6–TAM inhibition decreased fatal murine pulmonary embolism

Similarly, we evaluated the effects of UNC2025 in a collagen/epinephrine-induced PE model. Median survival time of saline-treated controls (2.5 min, IQR 2.0–3.1 min, $n = 27$) was shorter than that of mice treated with 3 mg kg^{-1} UNC2025 (15 min, IQR 1.6–15 min, $n = 16$, $P < 0.001$) (Fig. 5C). Fifty-six per cent of UNC2025-treated mice were alive 15 min after collagen/epinephrine injection, whereas all saline-treated controls developed fatal emboli in < 5 min. These data demonstrate UNC2025-mediated protection of mice from PE.

UNC2025 did not increase murine tail bleeding times

Significant differences in median bleeding times were not observed between saline-treated controls (6.2 min, IQR 5.9–8.5 min, $n = 8$) and mice treated with 3 mg kg^{-1} UNC2025 (5.9 min, IQR 4.8–8.5 min, $n = 3$) (Fig. 5D).

Combined antagonism of GAS6–TAM and ADP–P2Y$_{12}$ allows for inhibitor dose reduction in vivo

Similarly to the synergistic inhibition of platelet activation observed in aggregation assays, combined antagonism of P2Y and MERTK decreased thrombus formation *in vivo*. In the arterial thrombosis model, longer TTFO (Fig. 5A) was observed in mice treated with HD P2Yi (8.8 ± 0.6 min, $n = 5$, $P < 0.05$) or 3 mg kg^{-1} UNC2025 (8.4 ± 0.6 min, $n = 10$, $P < 0.05$) alone than in saline-treated controls (7.3 ± 0.6 min, $n = 19$). LD P2Yi-treated mice showed TTFO similar that of saline-treated controls (7.5 ± 0.2 min, $n = 5$, P = NS). Combining UNC2025 and the subtherapeutic LD P2Yi (9.9 ± 0.4 min, $n = 5$, $P < 0.05$), however, recapitulated the significantly longer TTFO caused by HD P2Yi.

Similarly, shorter DOO (Fig. 5B) was observed in mice treated with HD P2Yi (38.2 min, IQR 17.7–41.6 min,

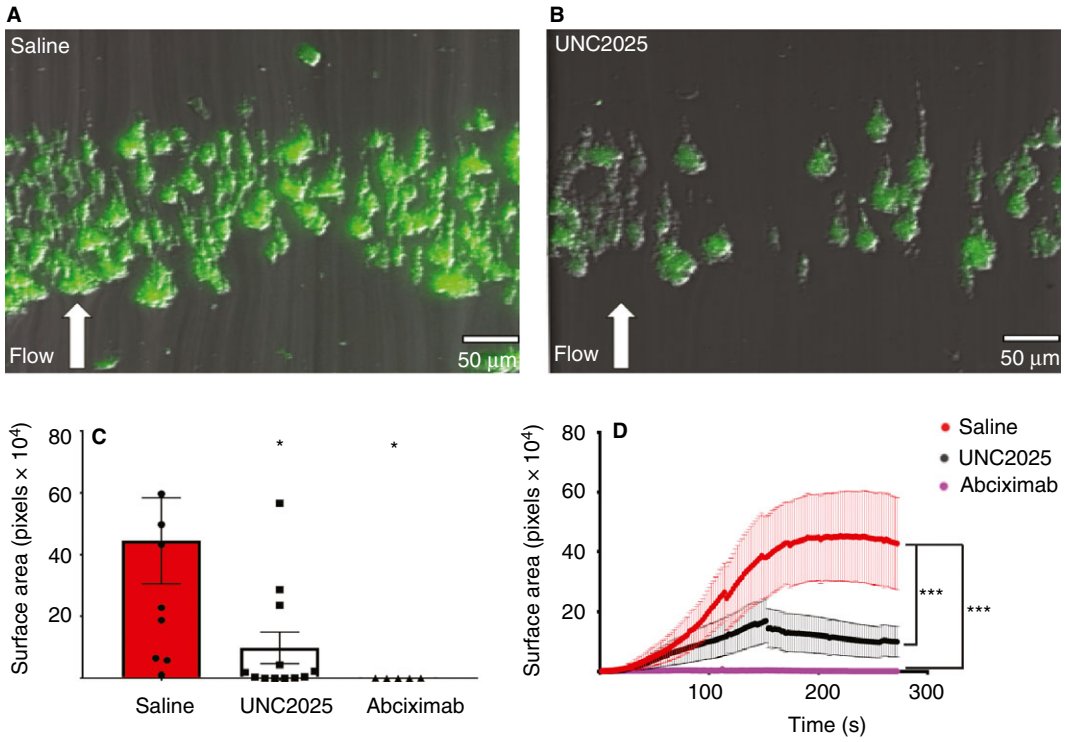

Fig. 3. UNC2025 decreases the stability of platelet aggregates under microfluidic physiologic flow conditions. (A, B) Fluorescein isothiocyanate-conjugated anti-CD41-labeled platelets in human whole blood were visualized following 3 min of perfusion at a shear rate of 650 s^{-1} across fibrillar collagen and a subsequent buffer rinse. Representative images demonstrate visibly decreased surface area coverage and aggregate size in samples pretreated with 1 μM UNC2025 (B) as compared with those pretreated with saline vehicle (A). (C) Quantification of surface area coverage after 5 min of flow. Mean values ± standard error were derived from 5–12 experiments performed with samples from five individual donors. Samples treated with 5 μM UNC2025 (black outlined bar) showed significantly decreased final surface area coverage relative to saline-treated controls (red), and a similar extent of final surface area coverage as the samples treated with the positive control abciximab (purple). Student's *t*-test: $*P < 0.05$. (D) Samples treated with 5 μM UNC2025 (black line) showed significantly less final surface area coverage and a delayed accumulation rate relative to saline-treated controls (red), and similar extents of these as samples treated with the positive control abciximab (purple). Mean values ± standard error from five independent donors are shown. Student's *t*-test: $***P < 0.0001$. [Color figure can be viewed at wileyonlinelibrary.com]

$P = 0.01$) or UNC2025 (38.2 min, IQR 9.9–50.1 min, $P = 0.02$) than in saline-treated controls (52.3 min, IQR 47.8–53.3 min). LD P2Yi-treated mice showed a DOO similar to that of saline-treated controls (52.9 min, IQR 52.4–52.9 min). Combining UNC2025 and LD P2Yi (41.3 min, IQR 14.5–46.8 min, $P = 0.03$) recapitulated the shorter DOO caused by HD P2Yi.

In the PE model (Fig. 5C) prolonged median survival was observed following collagen/epinephrine injection in mice treated with HD P2Yi (15.0 min, IQR 2.9–15.0 min, $n = 12$, $P < 0.001$) or UNC2025 (15.0 min, IQR 1.6–15.0 min, $n = 16$, $P < 0.001$) as compared with saline-treated controls (2.5 min, IQR 2.0–4.2 min, $n = 27$). Median survival was not significantly different in LD P2Yi-treated mice (6.9 min, IQR 2.2–15.0 min, $n = 5$), but treatment with the combination of UNC2025 and LD P2Yi (15.0 min, IQR 15.0–15.0 min, $n = 6$, $P < 0.0001$) recapitulated the longer survival caused by HD P2Yi. Sixty-eight per cent of HD P2Yi-treated mice ($P < 0.001$), 40% of LD P2Yi-treated mice (P = NS), 56% of UNC2025-treated mice ($P < 0.001$), and 90% of LD P2Yi + UNC2025-treated mice ($P < 0.0001$) were alive 15 min after collagen/epinephrine administration, whereas all saline-treated controls developed fatal emboli within 5 min. These data indicate that adding UNC2025 allows P2Yi dose reduction in murine models without compromising protection from arterial or venous thrombosis.

Mean (± SEM) tail bleeding times (Fig. 5D) were similar in mice pretreated with vehicle (6.4 ± 0.9 min, $n = 8$), UNC2025 (6.0 ± 1.2 min, $n = 3$, P = NS), LD P2Yi (6.5 ± 2.0 min, $n = 3$, P = NS), or LD P2Yi combined with UNC2025 (6.6 ± 2.7 min, $n = 3$, P = NS). Only HD P2Yi (12.9 ± 2.1 min, $n = 3$, $P < 0.05$) significantly prolonged bleeding.

Discussion

We show herein that pharmacologic inhibition of GAS6–TAM signaling efficiently abrogated platelet activation responses, leading to decreased aggregate stability and reduced thrombosis in animal models without increased bleeding. Additionally, we demonstrated a synergistic antiplatelet effect in the context of ADP–P2Y inhibition, consistent with a previous report suggesting that

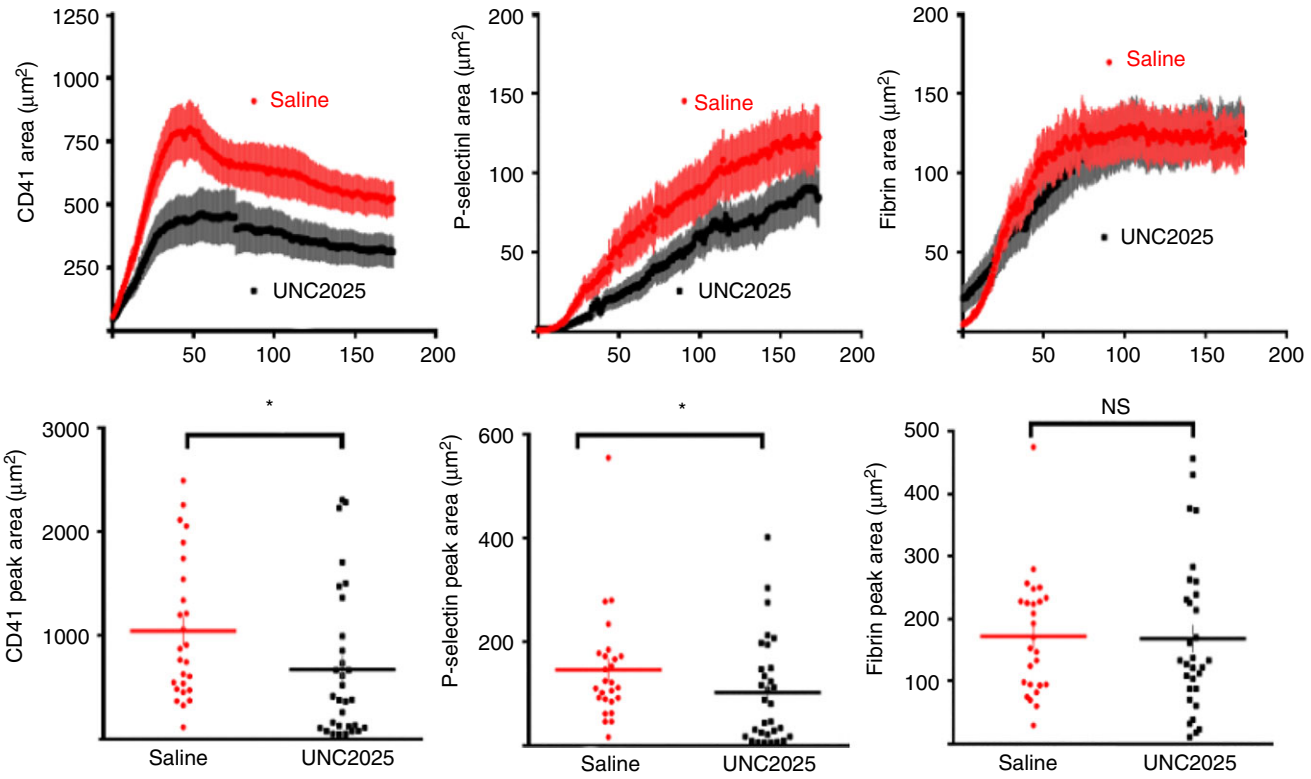

Fig. 4. UNC2025 decreases platelet accumulation in a microvascular thrombosis model. Total platelet accumulation, α-granule secretion and fibrin deposition were monitored following laser-induced injury in mouse cremaster arterioles, by the use of fluorescently tagged antibodies against mouse CD41, P-selectin, and fibrin, respectively. (A) Platelet accumulation (CD41-positive area), α-granule secretion (P-selectin-positive area) and fibrin deposition (fibrin area) over time in mice treated with 3 mg kg^{-1} UNC2025 (black line) or saline vehicle (red). Representative data from six mice are shown. (B) Median and interquartile range showing peaks of total platelet accumulation, P-selectin-positive platelet accumulation and fibrin accumulation areas in mice treated with 3 mg kg^{-1} UNC2025 (black dots) or saline (red dots). For vehicle, $n = 26$ thrombi, and for UNC2025, $n = 31$ thrombi, from six mice. Mann–Whitney test: $^*P < 0.05$, NS, not significant. [Color figure can be viewed at wileyonlinelibrary.com]

interruption of $\alpha_{IIb}\beta_3$ activation decreases the stability of platelet aggregates [44].

UNC2025 had antithrombotic and direct antiplatelet activity in a variety of *in vitro* and *in vivo* assays, both alone and in combination with P2Y inhibitors. UNC2025-treated platelets showed decreased activation in platelet aggregation assays, and reduced activity under physiologic shear stress. In the microfluidic assay, platelet adhesion to collagen in the first 60 s was not affected (Fig. 3D), but the binding of flowing platelets to collagen-adherent platelets was decreased, and large platelet aggregates dislodged more rapidly. These effects correlated with direct inhibiton of MERTK phosphorylation in platelets, and reduced downstream signaling through AKT and SRC (Fig. 1A,B), implicating MERTK inhibition as a mechanism of UNC2025-mediated functional effects. Additionally, the observed decrease in signaling of SRC, a known prothrombotic mediator in platelets [45] and a downstream target of TAM kinase signaling [46], suggests a biochemical mechanism by which TAM kinase inhibition mediates antithrombotic effects. However, a direct effect on SRC cannot be ruled out. It is of note that UNC2025 is equipotent against MERTK and FLT3, with 50-fold greater selectivity in cell-based assays than for AXL, the next most potently inhibited kinase [26]; however, FLT3 expression has not been reported in human or murine megakaryocytes or platelets, so the effects of treatment with UNC2025 are probably not mediated by FLT3 inhibition. Treatment with UNC2025 phenocopies the effects of genetic TAM kinase deletion in mouse platelets. Specifically, platelets from *Gas6*$^{-/-}$ and *Mertk*$^{-/-}$ mice show reduced aggregation *in vitro* and decreased clot stability *in vivo* [2–4], which are similar to the effects of UNC2025 reported here.

The similar inhibition of activation responses observed in both human and mouse platelets validates the use of UNC2025 for translational application in mouse models of thrombosis. The increased embolization that we noted in the microfluidic flow assay and arterial thrombosis model is reminiscent of the transient rebleeding after tail-clip in *Mertk*$^{-/-}$ mice noted previously [2], and is consistent with previous observations that *Gas6*$^{-/-}$ platelets form unstable aggregates under flow [5]. Whereas TTFO was minimally prolonged for inhibitor-treated mice, a significant difference was seen in the DOO between UNC2025-treated mice and controls. As the DOO is

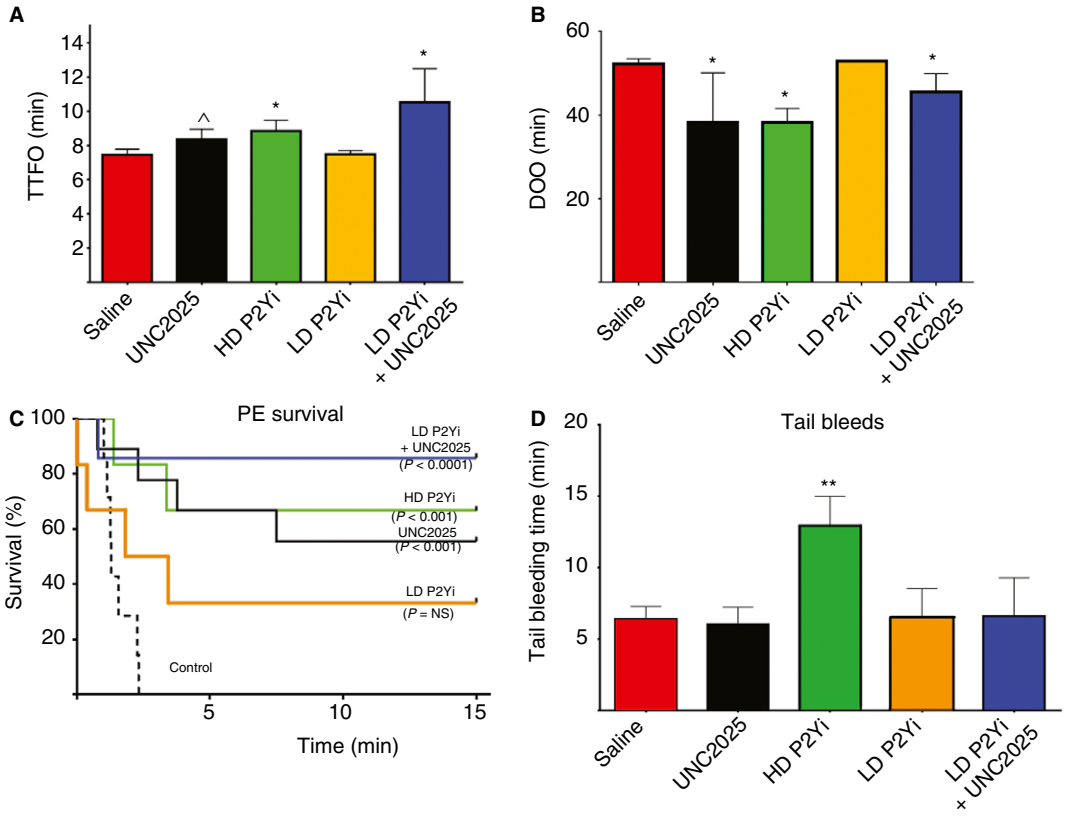

Fig. 5. UNC2025 synergizes with P2Y inhibitors and reduces drug dose requirements *in vivo*. Arterial and venous thrombosis models and tail bleed assays were conducted in mice treated with saline vehicle (red bars), 3 mg kg^{-1} UNC2025 (black bars), a high-dose $P2Y_1$ (MRS2179) and $P2Y_{12}$ (2-MeSAMP) inhibitor combination (HD P2Yi) (3 mg kg^{-1}, green), a low-dose $P2Y_1$ and $P2Y_{12}$ inhibitor combination (LD P2Yi) (1.5 mg kg^{-1}, orange) or LD P2Yi combined with UNC2025 (blue). Bar graphs depict medians (+ interquartile ranges). Synergy of the effects of P2Y inhibitors and of UNC2025 allow for statistically significant inhibition of thrombosis even at half the dose of P2Y inhibitors. (A) Following $FeCl_3$ application to the carotid artery of mice pretreated with HD P2Yi or UNC2025, the mice showed longer time to first occlusion (TTFO) than saline-treated controls. Mice pretreated with LD P2Yi showed TTFO similar to that of saline-treated controls. Combining UNC2025 and LD P2Yi, however, recapitulated the longer TTFO caused by HD P2Yi. (B) $FeCl_3$-induced thrombi had a shorter total duration of occlusion (DOO) in mice pretreated with HD P2Yi or UNC2025 than in saline-treated controls. Mice pretreated with LD P2Yi showed a DOO similar to that of saline-treated controls. Treatment with a combination of UNC2025 and LD P2Yi, however, recapitulated the longer DOO caused by HD P2Yi. (C) Significantly more mice pretreated with HD P2Yi, UNC2025 or LD P2Yi + UNC2025 than saline-treated controls remained alive 15 min after collagen/epinephrine injection. Pretreatment with LD P2Yi alone provided no survival advantage. (D) Tail bleeding time was significantly longer in HD P2Yi-treated mice than in saline-treated controls, but was not affected by treatment with LD P2Yi or UNC2025 administered alone or in combination. Statistics reflect comparison of each experimental condition with the vehicle control by use of the Mann–Whitney test: $^{\wedge}P = 0.05$, $*P < 0.05$, $**P < 0.01$. NS, not significant; PE, pulmonary embolism. [Color figure can be viewed at wileyonlinelibrary.com]

directly proportional to aggregate stability in this model, these results reflect relatively normal initial platelet adhesion and accumulation, but subsequent inability to stabilize aggregates in the setting of GAS6–TAM inhibition, consistent with what we observed *in vitro*. The results from the murine intravital laser-induced microvascular injury model demonstrated that GAS6–TAM inhibition decreases accumulation of activated (P-selectin-positive) platelets at injury sites by affecting platelet–platelet interactions, but not initial platelet adhesion or fibrin accumulation (a surrogate for thrombin activity). When considered in the context of hierarchical clot organization [40], these data suggest that GAS6–TAM inhibition may primarily affect the core of a newly formed clot. Although the *in vitro* experiments show that UNC2025 affects platelet function (human and murine) specifically, endothelial cells also express TAM receptors, and we cannot rule out a vascular effect of the compound *in vivo*. Future studies using transgenic models and transfused platelets will further elucidate any contribution of the vasculature to the observed phenotype.

UNC2025 also mediated a synergistic decrease in platelet aggregation in combination with an inhibitor of the ADP receptors $P2Y_1$ and $P2Y_{12}$ (P2Yi). This effect was recapitulated *in vivo* in the $FeCl_3$-induced arterial and PE thrombosis models, in which the addition of UNC2025 allowed for a 50% reduction in P2Yi dose without compromising thrombosis protection, consistent with prior

evidence of synergy between GAS6-evoked and ADP receptor inhibitor-evoked AKT phosphorylation [5]. Interestingly, inhibition of platelet aggregation and degranulation by MERTK antagonism can be overcome by high concentrations of ADP or thrombin receptor agonist peptide [6], and coinfusion of ADP can overcome the reduced aggregate formation under flow in *Gas6*$^{-/-}$, *Tyro3*$^{-/-}$ and *Axl*$^{-/-}$ mice [5], suggesting complementary roles for ADP–P2Y and GAS6–TAM signaling. Thus, combined GAS6–TAM and ADP–P2Y signaling is expected to mediate more effective inhibition of common downstream pathways, such as AKT and β_3 integrin, and our data support the idea that addition of a GAS6–TAM inhibitor to P2Yi treatment regimens could allow for P2Yi dose reduction, leading to a decreased risk of concomitant bleeding while maintaining the antithrombotic effect of HD P2Yi therapy [47,48]. In addition, owing to the moderate inhibition of platelet activation caused by UNC2025, GAS6–TAM inhibitors may be most useful as an adjunct to standard antiplatelet therapy, in a role similar to that considered for antithrombotic agents such as the protease-activated receptor 1 antagonist vorapaxar [49–51] or protein disulfide isomerase inhibitors [52].

Treatment with UNC2025 has been well tolerated in mice for up to 150 days, and the primary side effects associated with HD UNC2025 treatment were anemia and leukopenia [28]. These effects were not dose-limiting, and were probably primarily attributable to FLT3 inhibition in the bone marrow compartment. More extensive studies to assess the impact of MERTK inhibition on inflammation, infection and autoimmunity are needed to assess the potential consequences of long-term treatment with UNC2025.

In summary, GAS6–TAM pathway inhibition is an effective antithrombotic strategy in preclinical models, both alone and in combination with ADP–P2Y inhibitors. In addition, our data demonstrate therapeutic activity mediated by a novel translational agent without increased bleeding, and support the continued development of GAS6–TAM inhibitors for clinical applications where they may be useful in the context of short-term treatment when reduction of bleeding risk is imperative, such as prothrombotic surgical procedures, pulmonary vein ablation, and stent placement.

Addendum

B. R. Branchford designed and performed experiments, and analyzed/synthesized data. T. J. Stalker designed and performed experiments, analyzed/synthesized data, and reviewed/edited the manuscript. L. Law performed experiments, analyzed/synthesized data, and reviewed the manuscript. G. Acevedo performed experiments, analyzed/synthesized data, and reviewed the manuscript. S. Sather designed and performed experiments, analyzed/synthesized data, and reviewed the manuscript. C. Brzezinski performed experiments, analyzed/synthesized data, and reviewed the manuscript. S. R. Lentz designed experiments, provided training and equipment, and reviewed/edited the manuscript. K. M. Wilson performed experiments, analyzed/synthesized data, and reviewed the manuscript. K. Minson performed experiments, analyzed/synthesized data, and reviewed the manuscript. W. Zhang designed and tested experimental compounds, and reviewed the manuscript. A. B. Lee-Sherick performed experiments, analyzed/synthesized data, and reviewed the manuscript. P. Davizon-Castillo performed experiments, analyzed/synthesized data, and reviewed the manuscript. C. Ng performed experiments, analyzed/synthesized data, and reviewed the manuscript. K. B. Neeves provided training and equipment, analyzed/synthesized data, and reviewed/edited the manuscript. X. Wang oversaw the design and testing of experimental compounds, and reviewed/edited the manuscript. S. V. Frye oversaw the design and testing of experimental compounds, and reviewed/edited the manuscript. H. Shelton Earp III oversaw the design and testing of experimental compounds, and reviewed/edited the manuscript. D. DeRyckere was responsible for the initial concept, experimental design, data analysis, and manuscript editing. L. F. Brass was responsible for the initial concept, experimental design, data analysis, and manuscript editing. D. K. Graham was responsible for the initial concept, experimental design, experimental oversight, data analysis, and manuscript editing. J. A. Di Paola was responsible for the initial concept, experimental design, data analysis, manuscript editing, and provision of equipment and laboratory space.

Acknowledgements

The authors wish to thank K. Allison for technical assistance.

This study was supported in part by the National Hemophilia Foundation/Baxter Clinical Research Fellowship (B. R. Branchford), an American Society of Hematology Scholar Award (B. R. Branchford), a CSL Behring/Professor Heimburger Award in Hemostasis (B. R. Branchford), the NIH K12HD068372-03 Child Health Research Career Development grant (B. R. Branchford), a Hemostasis & Thrombosis Research Society Mentored Research Award sponsored by Shire (B. R. Branchford), 5H30MC00008-20-00 HRSA/MCHB (B. R. Branchford), and the Postle Chair and NIHR01 HL084086 (J. A. Di Paola). This work was also supported by the University Cancer Research Fund and Federal Funds from the National Cancer Institute, National Institute of Health, under Contract HHSN261200800001E.

Disclosure of Conflict of Interests

D. K. Graham, D. DeRyckere, S. Sather, and H. S. Earp have filed patents on targeting of the Mer tyrosine kinase

as cancer therapy. X. Wang, W. Zhang, and S. V. Frye have filed patent applications on UNC2025. The other authors state that they have no conflict of interest.

Supporting Information

Additional Supporting Information may be found in the online version of this article:

Fig. S1. UNC2025. Chemical structure and pharmacokinetic properties of the experimental compound UNC2025.
Fig. S2. UNC2025 mediates dose-dependent inhibition of platelet aggregation in response to stimulation with multiple agonists.
Fig. S3. UNC2025 decreases collagen-induced aggregation in washed murine platelets.
Fig. S4. ADPis and UNC2025 mediate synergistic decreases in platelet aggregation.
Fig. S5. UNC2025 decreases *in vitro* platelet activation responses.
Video S1. Laser injury in mouse cremaster muscle arterioles.

References

1 De Miguel A, Ibanez B, Badimon JJ. Clinical implications of clopidogrel resistance. *Thromb Haemost* 2008; **100**: 196–203.
2 Angelillo-Scherrer A, Burnier L, Flores N, Savi P, DeMol M, Schaeffer P, Herbert JM, Lemke G, Goff SP, Matsushima GK, Earp HS, Vesin C, Hoylaerts MF, Plaisance S, Collen D, Conway EM, Wehrle-Haller B, Carmeliet P. Role of Gas6 receptors in platelet signaling during thrombus stabilization and implications for antithrombotic therapy. *J Clin Invest* 2005; **115**: 237–46.
3 Angelillo-Scherrer A, de Frutos PG, Aparicio C, Melis E, Savi P, Lupu F, Arnout J, Dewerchin M, Hoylaerts MF, Herbert M, Collen D, Dahlback B, Carmeliet P. Deficiency or inhibition of Gas6 causes platelet dysfunction and protects mice against thrombosis. *Nat Med* 2001; **7**: 215–21.
4 Chen CL, Li Q, Darrow AL, Wang YP, Derian CK, Yang J, de Garavilla L, Andrade-Gordon P, Damiano BP. Mer receptor tyrosine kinase signaling participates in platelet function. *Arterioscler Thromb Vasc Biol* 2004; **24**: 1118–23.
5 Cosemans JM, Van Kruchten R, Olieslagers S, Schurgers LJ, Verheyen FK, Munnix IC, Waltenberger J, Angelillo-Scherrer A, Hoylaerts MF, Carmeliet P, Heemskerk JW. Potentiating role of Gas6 and Tyro3, Axl and Mer (TAM) receptors in human and murine platelet activation and thrombus stabilization. *J Thromb Haemost* 2010; **8**: 1797–808.
6 Gould WR, Baxi SM, Schroeder R, Peng YW, Leadley RJ, Peterson JT, Perrin LA. Gas6 receptors Axl, Sky and Mer enhance platelet activation and regulate thrombotic responses. *J Thromb Haemost* 2005; **3**: 733–41.
7 Foley JH, Conway EM. Gas6 gains entry into the coagulation cascade. *Blood* 2013; **121**: 570–1.
8 Korshunov VA. Axl-dependent signalling: a clinical update. *Clin Sci (Lond)* 2012; **122**: 361–8.
9 Brown JE, Krodel M, Pazos M, Lai C, Prieto AL. Cross-phosphorylation, signaling and proliferative functions of the Tyro3 and Axl receptors in Rat2 cells. *PLoS ONE* 2012; **7**: e36800.
10 Kim S, Mangin P, Dangelmaier C, Lillian R, Jackson SP, Daniel JL, Kunapuli SP. Role of phosphoinositide 3-kinase beta in glycoprotein VI-mediated Akt activation in platelets. *J Biol Chem* 2009; **284**: 33763–72.
11 Moore SF, Hunter RW, Harper MT, Savage JS, Siddiq S, Westbury SK, Poole AW, Mumford AD, Hers I. Dysfunction of the PI3 kinase/Rap1/integrin alpha(IIb)beta(3) pathway underlies *ex vivo* platelet hypoactivity in essential thrombocythemia. *Blood* 2013; **121**: 1209–19.
12 Zhang G, Xiang B, Ye S, Chrzanowska-Wodnicka M, Morris AJ, Gartner TK, Whiteheart SW, White GC 2nd, Smyth SS, Li Z. Distinct roles for Rap1b protein in platelet secretion and integrin alphaIIbbeta3 outside-in signaling. *J Biol Chem* 2011; **286**: 39466–77.
13 Joo SJ. Mechanisms of platelet activation and integrin alphaIIbeta3. *Korean Circ J* 2012; **42**: 295–301.
14 Woulfe DS. Akt signaling in platelets and thrombosis. *Expert Rev Hematol* 2010; **3**: 81–91.
15 O'Brien KA, Stojanovic-Terpo A, Hay N, Du XP. An important role for Akt3 in platelet activation and thrombosis. *Blood* 2011; **118**: 4215–23.
16 Shattil SJ, Newman PJ. Integrins: dynamic scaffolds for adhesion and signaling in platelets. *Blood* 2004; **104**: 1606–15.
17 Linger RM, Keating AK, Earp HS, Graham DK. Taking aim at Mer and Axl receptor tyrosine kinases as novel therapeutic targets in solid tumors. *Expert Opin Ther Targets* 2010; **14**: 1073–90.
18 Ekman C, Stenhoff J, Dahlback B. Gas6 is complexed to the soluble tyrosine kinase receptor Axl in human blood. *J Thromb Haemost* 2010; **8**: 838–44.
19 Nakano T, Ishimoto Y, Kishino J, Umeda M, Inoue K, Nagata K, Ohashi K, Mizuno K, Arita H. Cell adhesion to phosphatidylserine mediated by a product of growth arrest-specific gene 6. *J Biol Chem* 1997; **272**: 29411–14.
20 Rajotte I, Hasanbasic I, Blostein M. Gas6-mediated signaling is dependent on the engagement of its gamma-carboxyglutamic acid domain with phosphatidylserine. *Biochem Biophys Res Commun* 2008; **376**: 70–3.
21 Lemke G, Rothlin CV. Immunobiology of the TAM receptors. *Nat Rev Immunol* 2008; **8**: 327–36.
22 Laurance S, Lemarie CA, Blostein MD. Growth arrest-specific gene 6 (gas6) and vascular hemostasis. *Adv Nutr* 2012; **3**: 196–203.
23 Robins RS, Lemarie CA, Laurance S, Aghourian MN, Wu J, Blostein MD. Vascular Gas6 contributes to thrombogenesis and promotes tissue factor up-regulation after vessel injury in mice. *Blood* 2013; **121**: 692–9.
24 Sather S, Kenyon KD, Lefkowitz JB, Liang XY, Varnum BC, Henson PM, Graham DK. A soluble form of the Mer receptor tyrosine kinase inhibits macrophage clearance of apoptotic cells and platelet aggregation. *Blood* 2007; **109**: 1026–33.
25 van der Meer JH, van der Poll T, van't Veer C. TAM receptors, Gas6 and protein S: roles in inflammation and hemostasis. *Blood* 2014; **123**: 2460–9.
26 Zhang W, DeRyckere D, Hunter D, Liu J, Stashko MA, Minson KA, Cummings CT, Lee M, Glaros TG, Newton DL, Sather S, Zhang D, Kireev D, Janzen WP, Earp HS, Graham DK, Frye SV, Wang X. UNC2025, a potent and orally bioavailable MER/FLT3 dual inhibitor. *J Med Chem* 2014; **57**: 7031–41.
27 Cummings CT, Zhang W, Davies KD, Kirkpatrick GD, Zhang D, DeRyckere D, Wang X, Frye SV, Earp HS, Graham DK. Small molecule inhibition of MERTK is efficacious in non-small cell lung cancer models independent of driver oncogene status. *Mol Cancer Ther* 2015; **14**: 2014–22.
28 DeRyckere D, Lee-Sherick AB, Huey MG, Hill AA, Tyner JW, Jacobsen KM, Page LS, Kirkpatrick GG, Eryildiz F, Montgomery SA, Zhang W, Wang X, Frye SV, Earp HS, Graham DK. UNC2025, a MERTK small-molecule inhibitor, is therapeutically effective alone and in combination with methotrexate in leukemia models. *Clin Cancer Res* 2017; **23**: 1481–92.
29 McIver AL, Zhang W, Liu Q, Jiang X, Stashko MA, Nichols J, Miley MJ, Norris-Drouin J, Machius M, DeRyckere D,

Wood E, Graham DK, Earp HS, Kireev D, Frye SV, Wang X. Discovery of macrocyclic pyrimidines as MerTK-specific inhibitors. *ChemMedChem* 2017; **12**: 207–13.
30 McCarty OJ, Calaminus SD, Berndt MC, Machesky LM, Watson SP. von Willebrand factor mediates platelet spreading through glycoprotein Ib and alpha(IIb)beta3 in the presence of botrocetin and ristocetin, respectively. *J Thromb Haemost* 2006; **4**: 1367–78.
31 McCarty OJT, Larson MK, Auger JM, Kalia N, Atkinson BT, Pearce AC, Ruf S, Henderson RB, Tybulewicz VLJ, Machesky LM, Watson SP. Rac1 is essential for platelet Lamellipodia formation and aggregate stability under flow. *J Biol Chem* 2005; **280**: 39474–84.
32 Kastelowitz N, Tamura R, Onasoga A, Stalker TJ, White OR, Brown PN, Brodsky GL, Brass LF, Branchford BR, Di Paola J, Yin H. Peptides derived from MARCKS block coagulation complex assembly on phosphatidylserine. *Sci Rep* 2017; **7**: 4275.
33 Hansen RR, Wufsus AR, Barton ST, Onasoga AA, Johnson-Paben RM, Neeves KB. High content evaluation of shear dependent platelet function in a microfluidic flow assay. *Ann Biomed Eng* 2013; **41**: 250–62.
34 Neeves KB, Maloney SF, Fong KP, Schmaier AA, Kahn ML, Brass LF, Diamond SL. Microfluidic focal thrombosis model for measuring murine platelet deposition and stability: PAR4 signaling enhances shear-resistance of platelet aggregates. *J Thromb Haemost* 2008; **6**: 2193–201.
35 Neeves KB, Onasoga AA, Hansen RR, Lilly JJ, Venckunaite D, Sumner MB, Irish AT, Brodsky G, Manco-Johnson MJ, Di Paola JA. Sources of variability in platelet accumulation on type 1 fibrillar collagen in microfluidic flow assays. *PLoS ONE* 2013; **8**: e54680.
36 Naik MU, Stalker TJ, Brass LF, Naik UP. JAM-A protects from thrombosis by suppressing integrin alphaIIbbeta3-dependent outside-in signaling in platelets. *Blood* 2012; **119**: 3352–60.
37 Owens AP 3rd, Lu Y, Whinna HC, Gachet C, Fay WP, Mackman N. Towards a standardization of the murine ferric chloride-induced carotid arterial thrombosis model. *J Thromb Haemost* 2011; **9**: 1862–3.
38 Westrick RJ, Eitzman DT. Murine models of vascular thrombosis. *Arterioscler Thromb Vasc Biol* 2007; **27**: 2079–93.
39 Wilson KM, Lynch CM, Faraci FM, Lentz SR. Effect of mechanical ventilation on carotid artery thrombosis induced by photochemical injury in mice. *J Thromb Haemost* 2003; **1**: 2669–74.
40 Stalker TJ, Traxler EA, Wu J, Wannemacher KM, Cermignano SL, Voronov R, Diamond SL, Brass LF. Hierarchical organization in the hemostatic response and its relationship to the platelet-signaling network. *Blood* 2013; **121**: 1875–85.
41 Falati S, Patil S, Gross PL, Stapleton M, Merrill-Skoloff G, Barrett NE, Pixton KL, Weiler H, Cooley B, Newman DK, Newman PJ, Furie BC, Furie B, Gibbins JM. Platelet PECAM-1 inhibits thrombus formation *in vivo*. *Blood* 2006; **107**: 535–41.
42 Chou TC. Drug combination studies and their synergy quantification using the Chou–Talalay method. *Cancer Res* 2010; **70**: 440–6.
43 Branchford BR, Ng CJ, Neeves KB, Di Paola J. Microfluidic technology as an emerging clinical tool to evaluate thrombosis and hemostasis. *Thromb Res* 2015; **136**: 13–19.
44 Cosemans JM, Munnix IC, Wetzker R, Heller R, Jackson SP, Heemskerk JW. Continuous signaling via PI3K isoforms beta and gamma is required for platelet ADP receptor function in dynamic thrombus stabilization. *Blood* 2006; **108**: 3045–52.
45 Senis YA, Mazharian A, Mori J. Src family kinases: at the forefront of platelet activation. *Blood* 2014; **124**: 2013–24.
46 Lee-Sherick AB, Eisenman KM, Sather S, McGranahan A, Armistead PM, McGary CS, Hunsucker SA, Schlegel J, Martinson H, Cannon C, Keating AK, Earp HS, Liang X, DeRyckere D, Graham DK. Aberrant Mer receptor tyrosine kinase expression contributes to leukemogenesis in acute myeloid leukemia. *Oncogene* 2016; **35**: 6270.
47 Cattaneo M. New P2Y(12) inhibitors. *Circulation* 2010; **121**: 171–9.
48 Eikelboom JW, Hirsch J. Bleeding and management of bleeding. *Eur Heart J* 2006; **8**: G38–45.
49 Morrow DA, Braunwald E, Bonaca MP, Ameriso SF, Dalby AJ, Fish MP, Fox KAA, Lipka LJ, Liu X, Nicolau JC, Ophuis AJO, Paolasso E, Scirica BM, Spinar J, Theroux P, Wiviott SD, Strony J, Murphy SA, for the TRA 2P-TIMI 50 Steering Committee and Investigators. Vorapaxar in the secondary prevention of atherothrombotic events. *N Engl J Med* 2012; **366**: 1404–13.
50 Becker RC, Moliterno DJ, Jennings LK, Pieper KS, Pei J, Niederman A, Ziada KM, Berman G, Strony J, Joseph D, Mahaffey KW, Van de Werf F, Veltri E, Harrington RA, TRA-PCI Investigators. Safety and tolerability of SCH 530348 in patients undergoing non-urgent percutaneous coronary intervention: a randomised, double-blind, placebo-controlled phase II study. *Lancet* 2009; **373**: 919–28.
51 Tello-Montoliu A, Jover E, Rivera J, Valdes M, Angiolillo DJ, Marin F. New perspectives in antiplatelet therapy. *Curr Med Chem* 2012; **19**: 406–27.
52 Jasuja R, Passam FH, Kennedy DR, Kim SH, van Hessem L, Lin L, Bowley SR, Joshi SS, Dilks JR, Furie B, Furie BC, Flaumenhaft R. Protein disulfide isomerase inhibitors constitute a new class of antithrombotic agents. *J Clin Inves* 2012; **122**: 2104–13.